# Chapter 4. AlGaAs/GaAs Light-Emitting Devices on Si Substrates with Small Active Regions

## 4.1 Introduction

As described in chapters 2 and 3, it has been demonstrated that DLDs originating from the threading dislocations grew very rapidly with increasing injected current density for the GaAs-based lasers on Si[1]. It is believed that the failure of the lasers on Si is caused by the rapid DLD growth. Although many previous efforts have been mainly focused on the reduction of the dislocation density, it has not been realized that the dislocation density is reduced to a level at least below ~$10^4$ $cm^{-2}$ observed in the GaAs layer on a GaAs substrate.

If the sizes of active regions are drastically reduced, the number of dislocations in the active regions can be reduced[2]. Therefore, the reliability can be expected to be improved for the GaAs-based LEDs and lasers on Si with the small active regions.

Recently, Kapon and co-workers[3-5] have demonstrated the AlGaAs/GaAs lasers with GaAs quantum wire-like active regions by use of the regrowth technique of MOCVD on nonplanar GaAs substrates. The two-dimensional quantum confinement of injected carriers has also been observed from the optical properties of the quantum wire-like lasers[6-15]. Furthermore, the high-quality self-formed nanometer-scale GaAs and InGaAs quantum dot-like islands have been currently realized on GaAs substrates using the several growth techniques such as droplet-epitaxy[16,17], Stranski-Krastanow (SK) growth mode[18-26] and self-organizing growth mode on GaAs (311)B substrates[27-31]. The lasers with these islands in the active regions have been also fabricated[32-34].

In this chapter, the successful fabrications of vertically-stacked quasi GaAs quantum wires grown on a V-grooved GaAs/Si substrate[35] and self-formed GaAs islands grown by droplet-epitaxy on a GaAs/Si substrate[36] are described. These shapes and sizes were observed using a high-resolution SEM (HITACHI S-5000) and an AFM (SPI 3700/SPA-300). These GaAs structures were also applied to the active regions of an AlGaAs/GaAs laser and an LED on Si. This chapter is organized as follows: In section 4.2, fabrication of an AlGaAs/GaAs quantum wire-like laser on a V-grooved GaAs/Si substrate is described. Fabrication of an AlGaAs/GaAs LED on Si with self-formed GaAs islands active region is presented in section 4.3. This chapter is concluded in section 4.4.

## 4.2 AlGaAs/GaAs Quantum Wire-Like Lasers on V-Grooved GaAs/Si Substrates

### 4.2.1 Vertically-Stacked Quasi GaAs Quantum Wires

Figure 4.1 shows the flowchart of the fabrication process for an AlGaAs/GaAs quantum wire-like laser on a V-grooved GaAs/Si substrate. In the first growth, an initial 10-nm-thick undoped GaAs nucleation layer and a 2.5-μm-thick $n^+$-GaAs buffer layer were grown on an $n^+$-Si substrate [Fig. 4.1(a)]. During growth of the $n^+$-GaAs layer, thermal cycle annealing was performed five times by varying the substrate temperature between 350 and 850 °C in an $AsH_3$ atmosphere. Next, V-shaped grooves with depth of ~1.2 μm and width of ~2.7 μm were formed with a 300 μm pitch along the [011] direction on a (100) GaAs/Si substrate using photolithography and wet chemical etching techniques [Fig. 4.1(b)]. As a reference, a GaAs/Si substrate with U-shaped grooves with depth of ~0.7 μm, top-width of ~2.7 μm and bottom-width of ~1.0 μm was also prepared. The chemical

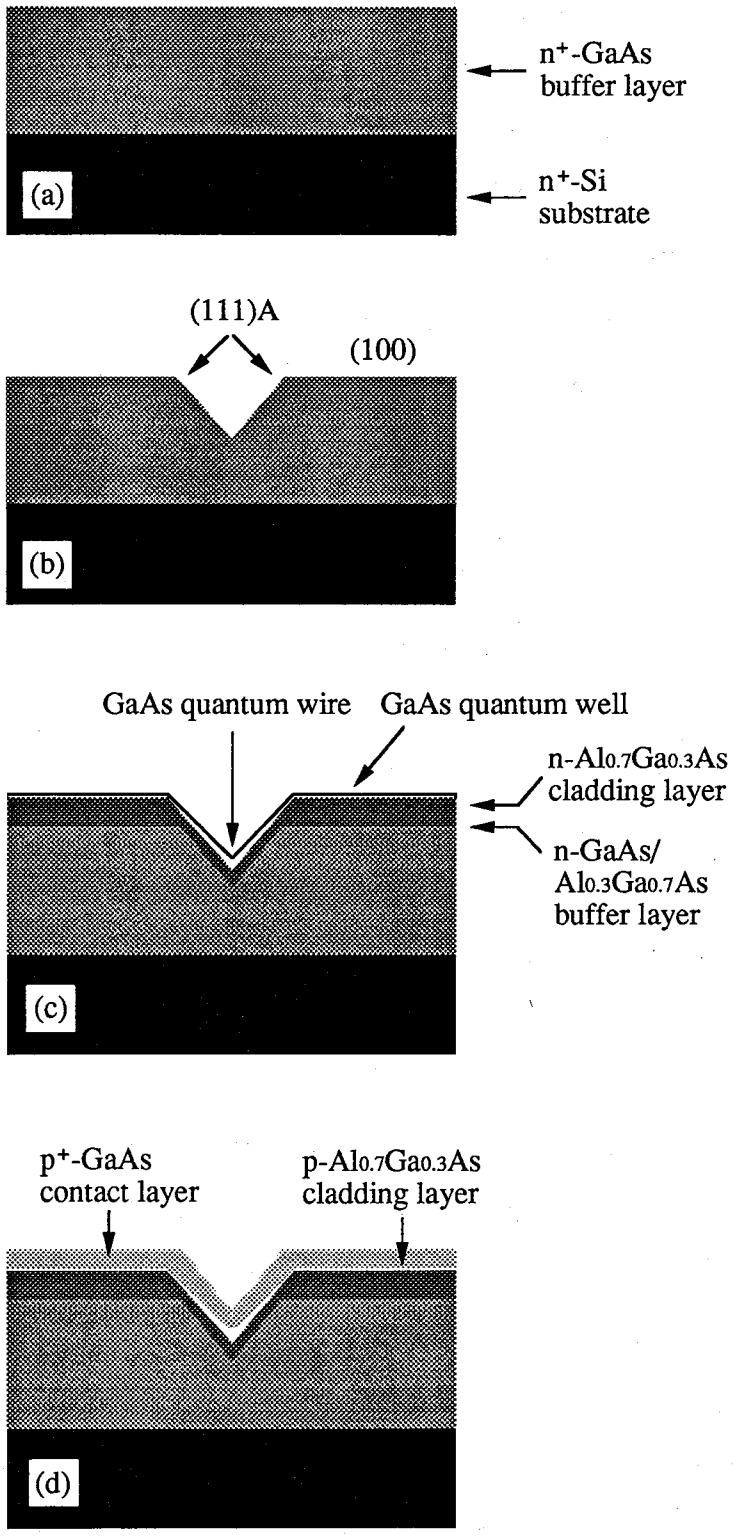


Fig. 4.1. Flowchart of the fabrication process for an AlGaAs/GaAs quantum wire-like laser on a V-grooved GaAs/Si substrate.

etching in a solution of $H_2SO_4$ : $H_2O_2$ : $H_2O$ (1 : 8 : 40 by volume) forms the V and U-grooves with (111)A side-walls[37]. The V-grooved substrate was then etched in a solution of $H_2SO_4$ : $H_2O_2$ : $H_2O$ (4 : 1 : 1 by volume) in order to create the round corner at the bottom of the V-groove. After the photoresist mask was removed, the substrates were stored in methyl alcohol. The grooved substrates were then cleaned in HCl and loaded into the reactor for the second growth. For the second growth, the AlGaAs/GaAs laser structure was grown on both V- and U-grooved GaAs/Si substrates by MOCVD. The structure consisted of a 10-nm-thick $n^+$-GaAs buffer layer, five periods of a 10-nm-thick $n^+$-GaAs/10-nm-thick $n^+$-$Al_{0.3}Ga_{0.7}As$ buffer superlattice, a 0.51-μm-thick n-$Al_{0.7}Ga_{0.3}As$ lower cladding layer, a 60-nm-thick undoped $Al_{0.3}Ga_{0.7}As$ lower confining layer, three 3-nm-thick undoped GaAs quantum wells separated by 5.5-nm-thick undoped $Al_{0.3}Ga_{0.7}As$ barrier layers, a 60-nm-thick undoped $Al_{0.3}Ga_{0.7}As$ upper confining layer, a 0.51-μm-thick p-$Al_{0.7}Ga_{0.3}As$ upper cladding layer and a 0.1-μm-thick $p^+$-GaAs contact layer [Figs. 4.1(c) and 4.1(d)]. Thickness of each layer was determined from GaAs and AlGaAs growth rates on a planar substrate. After the growth, the samples were cleaved perpendicular to the direction of the grooves for the high-resolution SEM observation.

Figure 4.2 shows a cross-sectional SEM micrograph of the overall AlGaAs/GaAs quantum wire-like laser grown on a V-grooved GaAs/Si substrate. The active layers of this laser are sharply defined along the V-groove with (111)A side-walls. Near the center of the V-groove, a (100) bottom surface is bounded between the two (111)A side-walls. No cracks were observed at the center of the V-grooves. This result indicates that relaxation of the large residual thermal stress in the GaAs/Si did not occur after forming the V-grooves or during cooling from the growth temperature (750 °C)

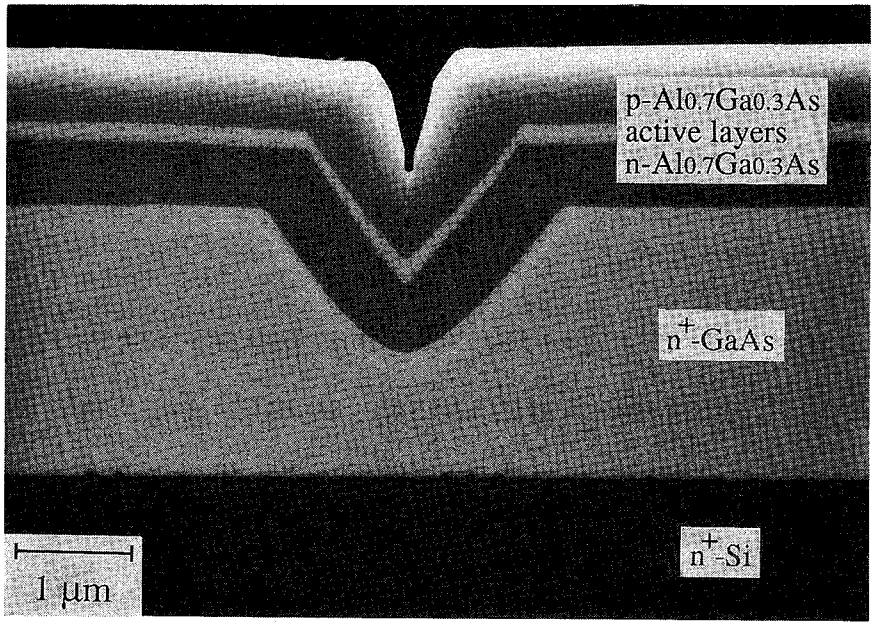


Fig. 4.2. Cross-sectional SEM micrograph of the overall AlGaAs/GaAs quantum wire-like laser on a V-grooved GaAs/Si substrate.

to room-temperature in the second growth. Figures 4.3(a) and 4.3(b) show a cross-sectional magnified SEM micrograph and a schematic diagram of the vertically-stacked quasi GaAs quantum wires near the center of the V-groove in Fig. 4.2, respectively. As shown in Fig. 4.3(a), the crescent-shaped quasi GaAs quantum wires of size (11-15 nm thick at its center)×(83-127 nm wide) are successfully grown on the V-grooved GaAs/Si substrate. They are realized by Ga atom accumulation from (111)A side-walls to the (100) bottom surface of the V-groove[10]. However, nonuniformity among each quantum wire can also be seen. In going from the first (bottom) to the third (top) quantum wire, the lateral width of each quantum wire is increased and the vertical thickness is decreased. The reason may be that the 5.5-nm-thick $Al_{0.3}Ga_{0.7}As$ barrier layers are too thin to recover the larger curvature of the center of the subsequently grown quantum wires[10,13,15]. Another significant result is that each quantum wire seems to be independent of the quantum well grown on the (111)A side-walls, which results in the formation of quantum wires of a small size. This indicates that this quantum wire-like laser has a much attractive advantage of low dislocation number arising from the reduction in the size of the active region. For example, assuming that the dislocation density is $1\times10^7$ $cm^{-2}$, the dislocation number of this quantum wire-like laser with 300-μm-long cavity is estimated to be ~3, while that of the conventional quantum well laser on Si with 10-μm-wide stripe contact window and 300-μm-long cavity (shown in Fig. 2.1) are ~300. This reduction of dislocations contributes to the suppression of rapid degradation for GaAs-based lasers on Si.

Additionally, the growth of quantum wells on a U-grooved GaAs/Si substrate have been also studied. The overall AlGaAs/GaAs laser structure grown on the U-grooved substrate is shown in Fig. 4.4(a). The active layers of this laser do not seem to be sharply

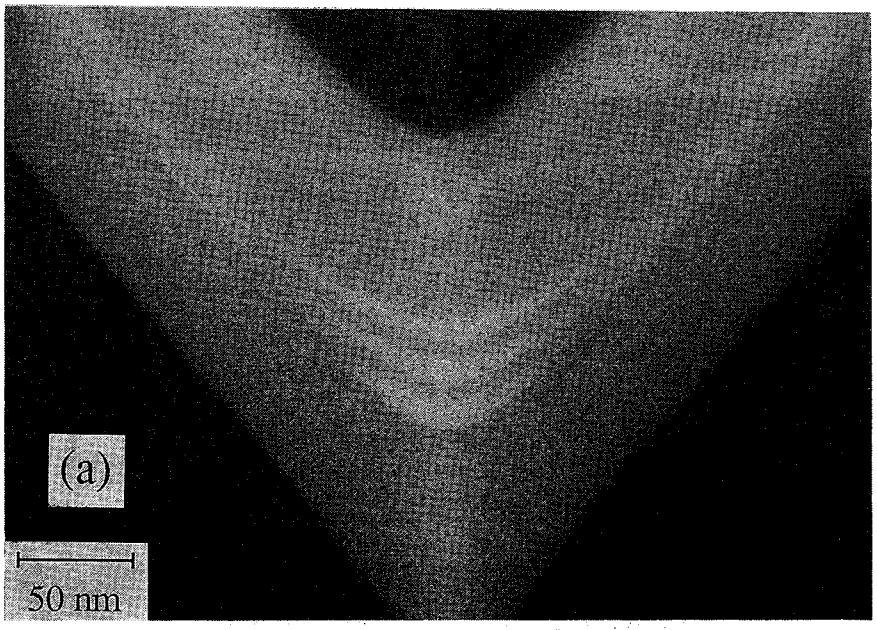


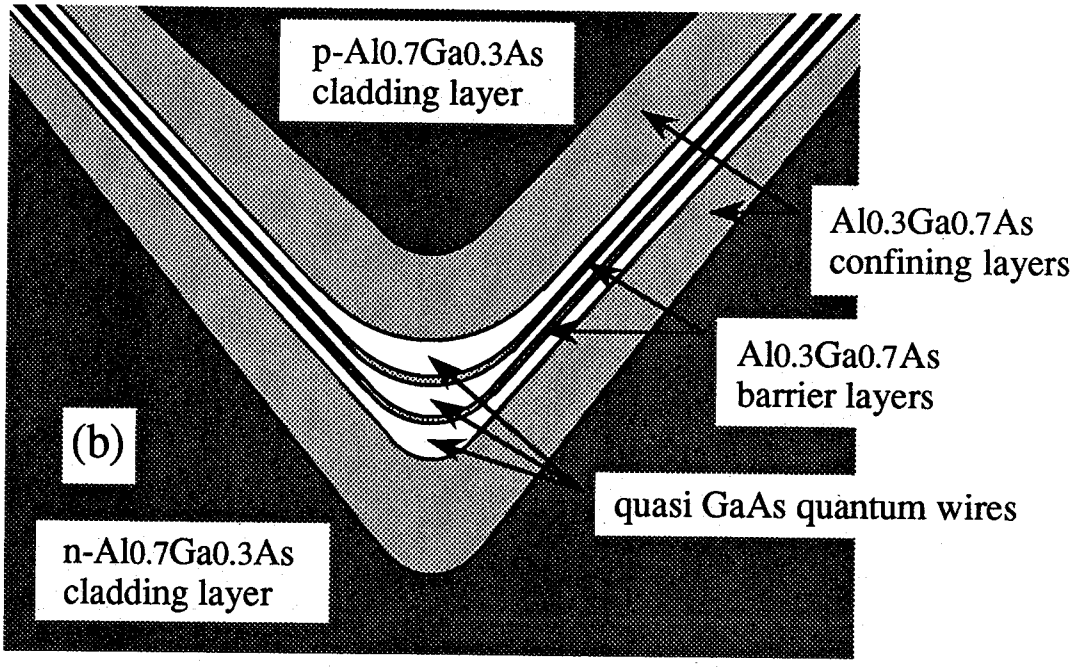


Fig. 4.3. Cross-sectional image of the vertically-stacked quasi GaAs quantum wires of size (11-15 nm)×(83-127 nm) near the center of the V-groove in Fig. 4.2: (a) magnified SEM micrograph and (b) schematic diagram.

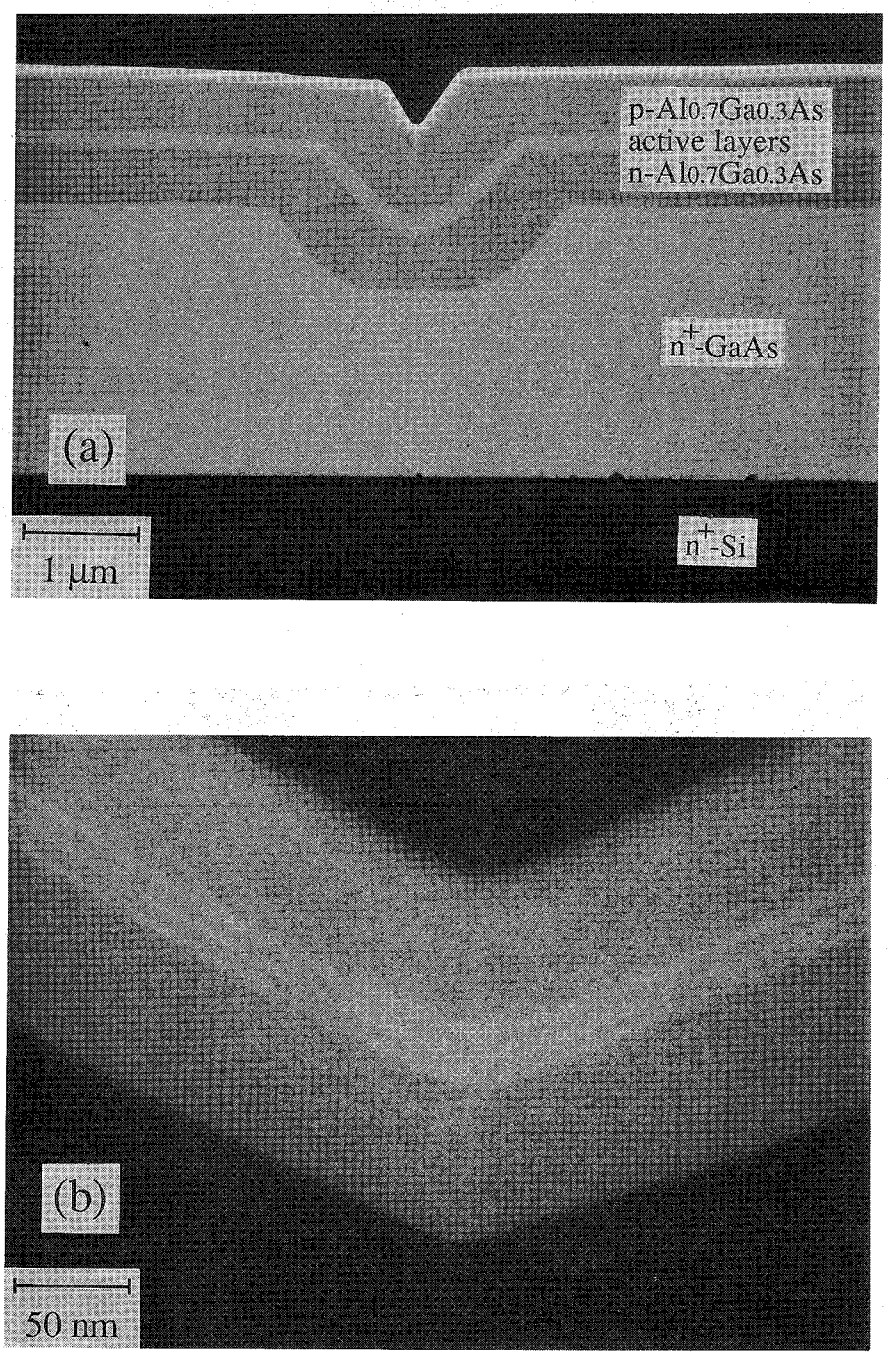


Fig. 4.4. Cross-sectional SEM micrographs: (a) overall AlGaAs/GaAs patterned quantum well laser on a U-grooved GaAs/Si substrate and (b) vertically-stacked GaAs patterned quantum wells near the center of the U-groove.

formed along the U-groove which has a (100) bottom surface and (111)A side-walls. Figure 4.4(b) shows the vertically-stacked GaAs patterned quantum wells near the center of the U-groove in Fig. 4.4(a). The crescent-shaped GaAs quantum wires seen in Fig. 4.3(a) are not formed on the U-grooved substrate because another new facet in addition to the (111)A appears near the center of the U-groove. This new facet is thought to be (311)A by the measurement of the angle from the SEM micrograph of Fig. 4.4(b). This results in the formation of GaAs patterned quantum wells on the U-grooved substrate and indicates that the sharp V-groove with (111)A side-walls plays an important role in the successful formation of GaAs quantum wires.

### 4.2.2 Lasing Characteristics

The extremely low-threshold characteristics of an AlGaAs/GaAs laser with the vertically-stacked quasi GaAs quantum wires of size (20-21 nm) × (100-260 nm) grown on a V-grooved GaAs/Si substrate were also demonstrated[38-40]. This quantum wire-like laser has been fabricated by the growth of three 9-nm-thick GaAs quantum wells and a $p^+$-GaAs current-blocking layer. Laser devices were fabricated as follows: A 0.1-μm-thick $SiO_2$ insulating layer was deposited on the $p^+$-GaAs contact layer and 2-μm-wide stripe contact windows were opened just on the grooves by wet chemical etching of $SiO_2$ in order to confine the injected current. Ti/Au was then evaporated on the $p^+$-GaAs layer as the p-contact. After thinning the $n^+$-Si substrate to a thickness of ~100 μm, AuSb/Au was evaporated on the Si substrate to form the n-contact. In order to reduce the series resistance, the contacts were annealed in a $N_2$ atmosphere at 380 °C. The samples were then cleaved into chips and mounted on In soldered Cu heatsinks in the p-side-up configuration. This quantum wire-like laser was tested at room-temperature under pulsed (0.2 μs pulses at

5 kHz repetition rate) and cw conditions.

Figures 4.5(a) and 4.5(b) show a cross-sectional SEM micrograph of the overall AlGaAs/GaAs quantum wire-like laser on Si with the $p^+$-GaAs current-blocking layer and a schematic diagram of the injected current distribution, respectively. As shown in Fig. 4.5(a), a 1.6-μm-thick $n^+$-GaAs and a 1.0-μm-thick $p^+$-GaAs (Zn-doped, $1\times10^{19}$ $cm^{-3}$) layers were grown on a Si as a GaAs buffer layer. Figure 4.5(b) shows that the $p^+$-GaAs layer acts as an internal current-blocking layer and prevents the current leakage path outside the V-groove. This internal current blocking is provided by the p-n-p-n junction structure outside the V-groove. However, the process of $SiO_2$ opening just on the V-groove must be carefully carried out, because the $SiO_2$ on both edges of the groove are easily removed and the light can be emitted at these edges due to the current leakage path.

Figure 4.6 shows the I-V characteristics of this quantum wire-like laser outside the V-groove with a $p^+$-GaAs current-blocking layer and inside the V-groove without the layer. The turn-on voltage was 1.2 V without the current-blocking layer. On the other hand, no current flow was observed with the layer up to 5 V. This result indicates that the $p^+$-GaAs layer is useful enough to confine the injected current into the quantum wires near the center of the V-groove.

Figure 4.7 shows the L-I characteristic and the emission spectrum of this quantum wire-like laser under pulsed condition at room-temperature. A pulsed $I_{th}$ as low as 9.8 mA was obtained for the 123-μm-long laser. The value of $\eta_d$ was 21 %. The peak emission wavelength was 858 nm at $2.0\times I_{th}$. In addition, the laser beam was mainly polarized parallel to the (100) substrate plane (TE-like mode). In order to compare the lasing characteristics, a

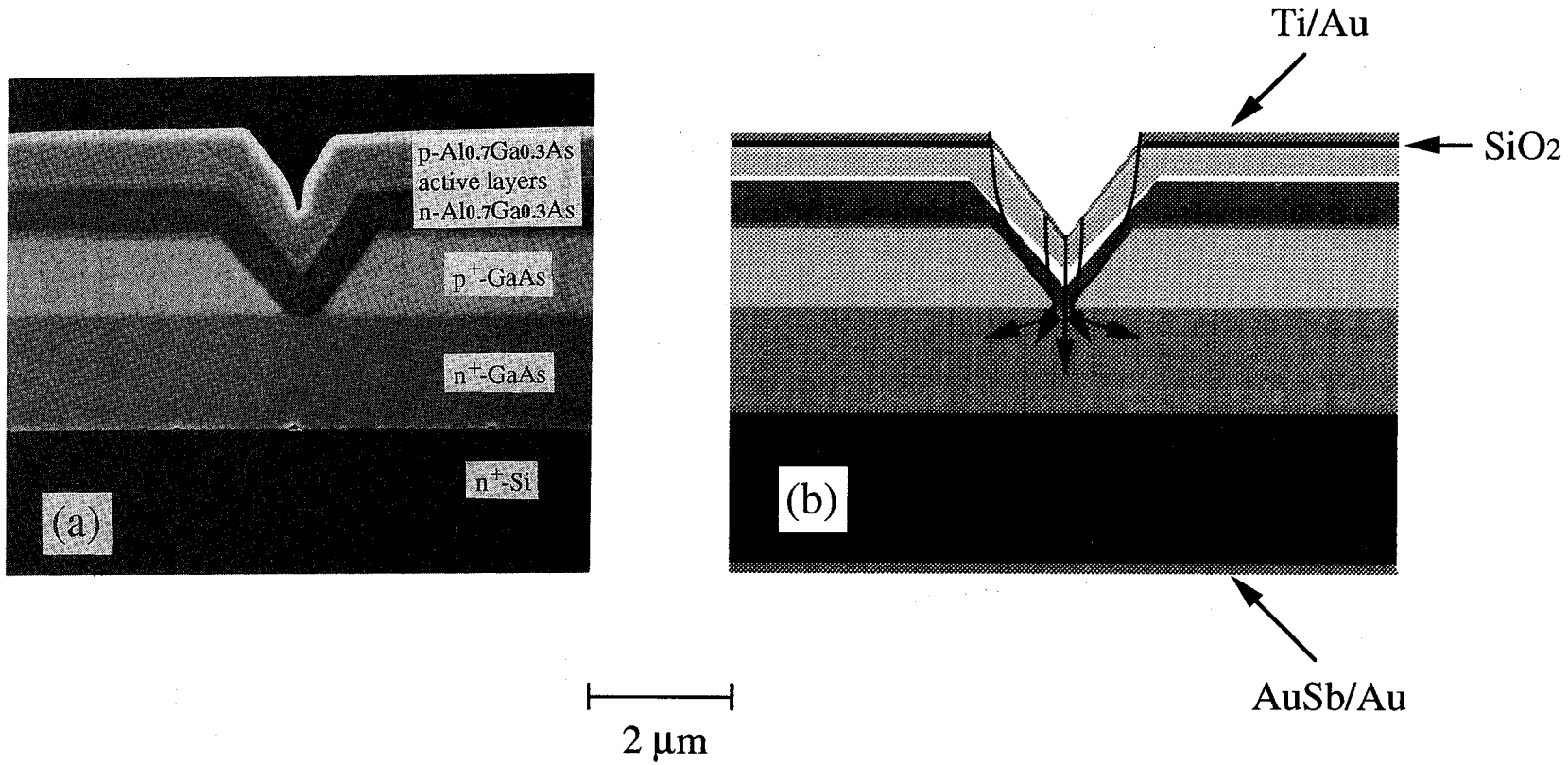


Fig. 4.5. Cross-sectional image of the overall AlGaAs/GaAs quantum wire-like laser on Si with $p^+$-GaAs current-blocking layer: (a) SEM micrograph and (b) schematic diagram of the injected current distribution.

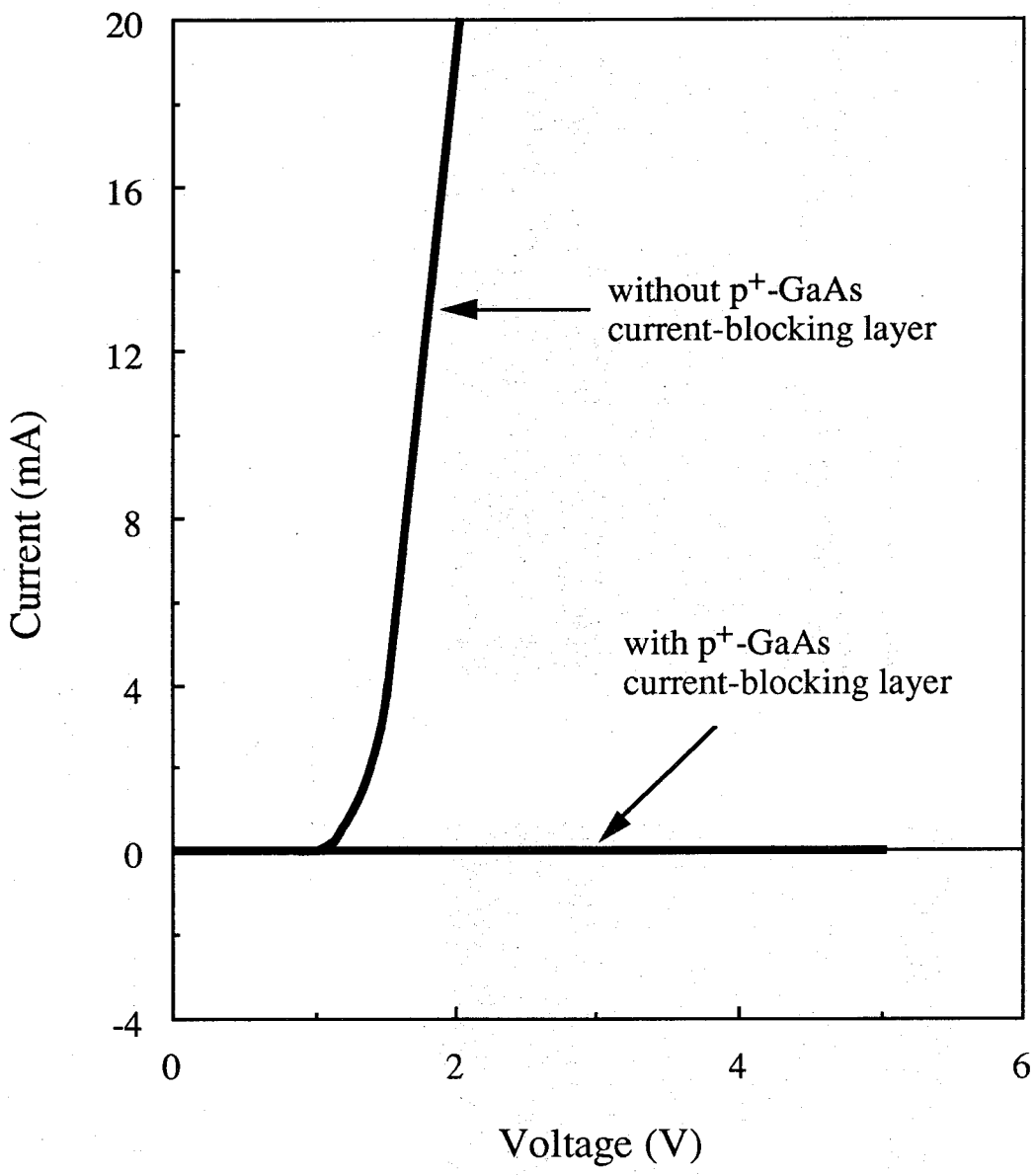


Fig. 4.6. I-V chracteristics of the quantum wire-like laser on Si outside the V-groove with $p^+$-GaAs current-blocking layer and inside the V-groove without the layer.

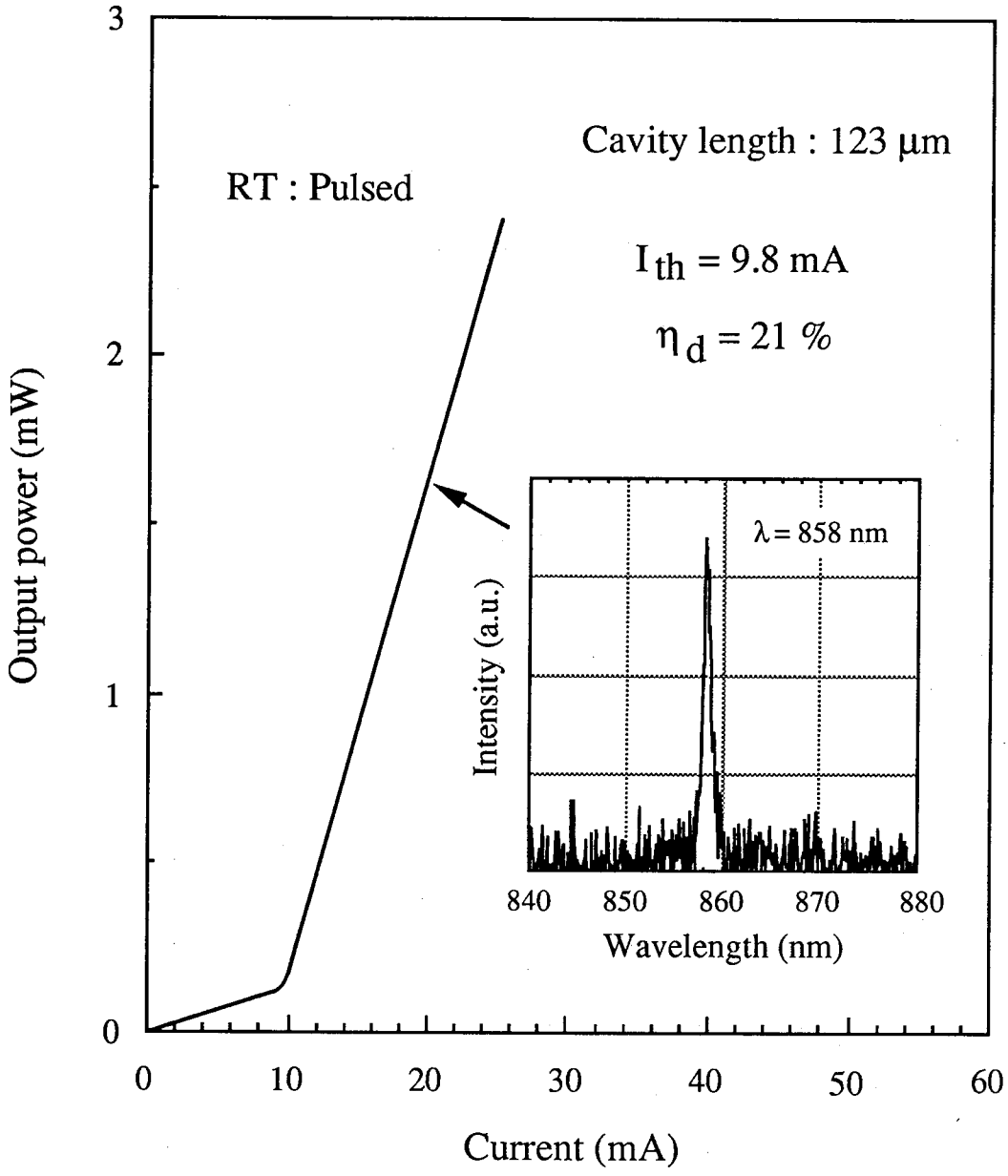


Fig. 4.7. L-I characteristic and emission spectrum of the quantum wire-like laser on Si under pulsed condition at room-temperature.

conventional AlGaAs/GaAs quantum well laser grown on a planar GaAs/Si substrate with three 9-nm-thick GaAs quantum wells and a 2-μm-wide stripe contact window was prepared. Under cw operation, the distribution of $I_{th}$ against cavity length for the quantum wire-like lasers and the conventional quantum well lasers on Si were measured. The minimum $I_{th}$ was 24-64 mA for the quantum well laser cavities of length 100-380 μm. For the quantum wire-like lasers, $I_{th}$ was as low as 16-20 mA for cavities of length 150-380 μm. In particular, to date, a pulsed $I_{th}$ of 9.8 mA and a cw $I_{th}$ of 16 mA for the quantum wire-like lasers are the lowest values so far reported for conventional quantum well lasers on Si[41-47]. The improvement in $I_{th}$ is thought to have been achieved by employing quantum wire structures with a reduction in the size of the active region.

## 4.3 AlGaAs/GaAs LEDs on Si with Self-Formed GaAs Islands Active Regions

### 4.3.1 Self-Formed GaAs Islands on GaAs/Si Substrates

A 2.5-μm-thick thermal-cycle annealed $n^+$-GaAs buffer layer was grown on an $n^+$-Si substrate by the two-step growth technique. The growth temperature was 750 °C except for the initial 10-nm-thick undoped GaAs nucleation layer which was grown on Si at 400 °C. In the preliminary experiment, the GaAs islands were grown on the $n^+$-GaAs/Si substrate at 700 °C using droplet-epitaxy[17] by the supply of TMG and successive $AsH_3$ supply. At the same time, the GaAs islands were also grown side-by-side on an $n^+$-GaAs (100) substrate as a reference. Figure 4.8 shows the typical supply sequence of TMG and $AsH_3$ for droplet-epitaxy. The details about growth sequence of this droplet-epitaxy is as follows: After the substrate temperature reached the growth temperature at 700 °C, the $AsH_3$ flow was stopped.

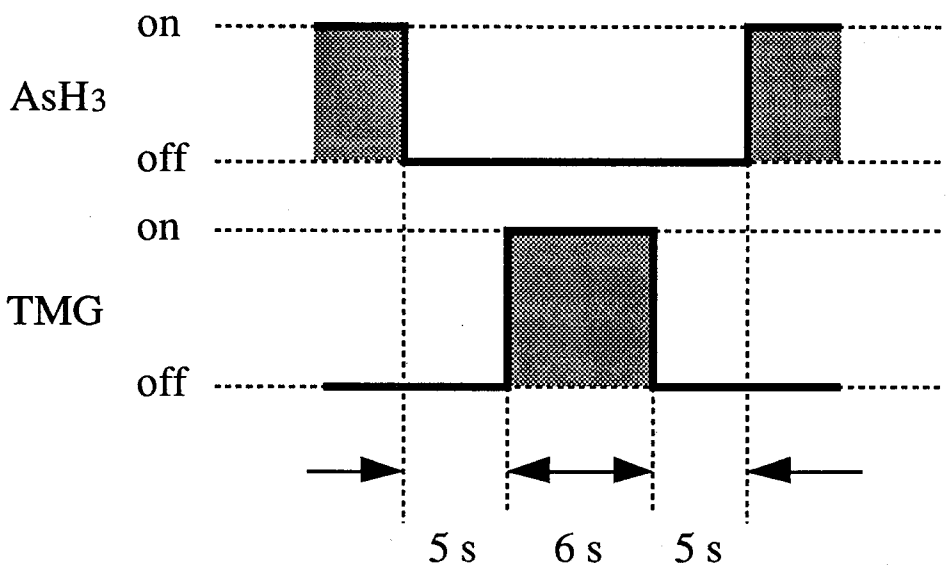


Fig. 4.8. Typical supply sequence of TMG and $AsH_3$ for droplet-epitaxy.

5 s later, the TMG was supplied for 6 s. Ga droplets were formed at this stage. The $AsH_3$ was supplied again with 5 s interval after stopping the TMG supply. At this stage, the Ga droplets were transformed to GaAs islands. This growth mechanism is believed to be similar to the vapor-liquid-solid (VLS) equilibrium phase growth model[48-50]. Using an AFM, the self-formed GaAs islands on the GaAs/Si substrate were observed as shown in Fig. 4.9. In this experiment, the TMG flow rate and time were 10 sccm and 6 s, respectively. This growth condition corresponds to a 5-nm-thick GaAs layer by the simultaneous supply of TMG and $AsH_3$. It can be seen that the GaAs islands on the GaAs/Si are randomly formed as well as the islands on the GaAs substrate in spite of the surface roughness (~20 nm) of the GaAs layer on Si[51]. The islands exhibited the conical shape with the heights of 90-170 nm, the effective diameters of 600-750 nm and the density of $1\text{-}2\times10^7$ $cm^{-2}$. It was also observed that the islands aligned on the cracks of GaAs/Si. This self-alignment of the islands seems to be caused by the Ga droplet accumulation on the bottom of the cracks. In addition, the size and density of self-formed GaAs islands could be controlled by the growth condition such as the TMG flow rate. Figures 4.10(a) and 4.10(b) show the dependence of island size and density on the TMG flow rate. The TMG flow time was kept constant at 6 s. As shown in Fig. 4.10(a), the island height decreases with the increase of the TMG flow rate, while the diameter increases with increasing the TMG flow rate. Figure 4.10(b) shows that the island density can be controlled between $10^6$ and $10^7$ $cm^{-2}$ by varying the TMG flow rate, which results from increasing density of the Ga dimer of critical nucleus with the increase of TMG flow rate.

### 4.3.2 L-I Characteristics

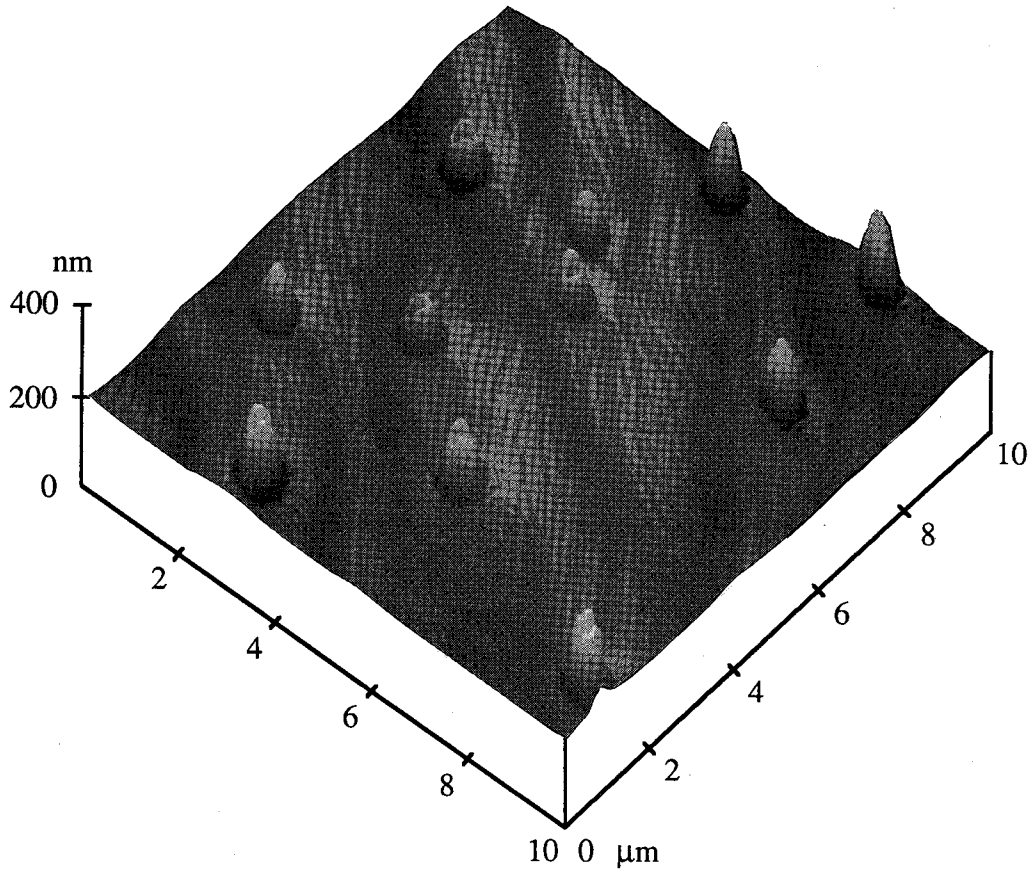


Fig. 4.9. AFM image of the self-formed GaAs islands on GaAs/Si substrate. The TMG flow rate and time were 10 sccm and 6 s, respectively.

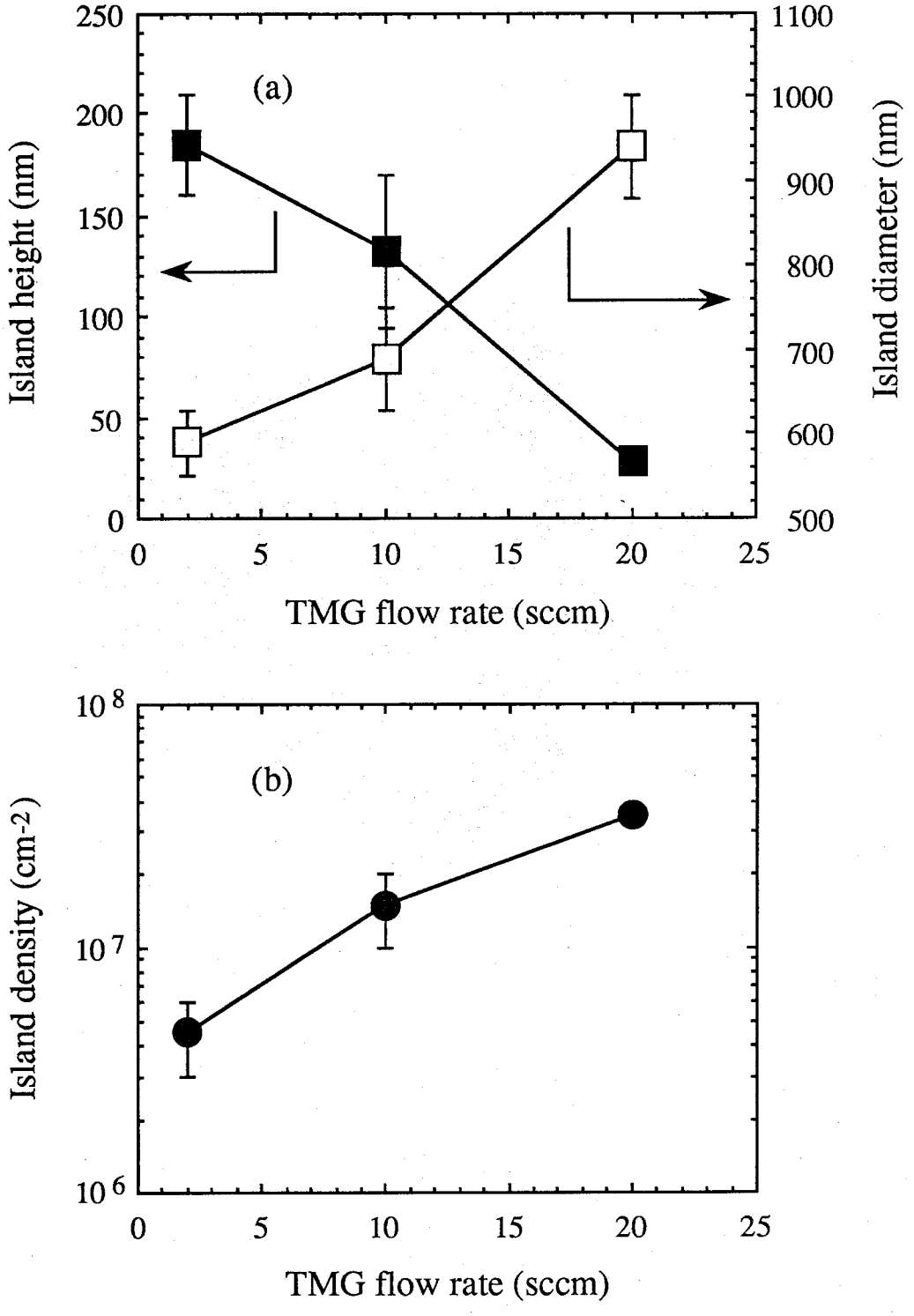


Fig. 4.10. Dependence of (a) island size and (b) island density on the TMG flow rate. The TMG flow time was kept constant at 6 s.

Figures 4.11(a) and 4.11(b) show cross-sectional SEM micrographs of the overall LED on Si and the magnified GaAs islands active region, respectively. The LED structure comprised a 2.5-μm-thick thermal-cycle annealed $n^+$-GaAs buffer layer, a 0.74-μm-thick n-$Al_{0.7}Ga_{0.3}As$ lower cladding layer, a 70-nm-thick undoped $Al_{0.3}Ga_{0.7}As$ lower confining layer, undoped GaAs islands active region formed by droplet-epitaxy, a 70-nm-thick undoped $Al_{0.3}Ga_{0.7}As$ upper confining layer and a 0.74-μm-thick p-$Al_{0.7}Ga_{0.3}As$ upper cladding layer. An 80-nm-thick $p^+$-GaAs contact layer was finally grown. After the growth, surface-emitting LED was fabricated from this wafer by depositing Ti/Au contact ring as the p-side electrode. AuSb/Au were evaporated on the $n^+$-Si substrate as the n-side electrode. During the droplet-epitaxy in the LED growth, the TMG flow rate and time were 10 sccm and 6 s, respectively. This growth condition is the same as that shown in Fig. 4.9. As shown in Fig. 4.11(a), it is found that two bright areas in $Al_{0.3}Ga_{0.7}As$/GaAs region are GaAs islands. The island is connected to some extent with a very thin GaAs layer at the interface of the $Al_{0.3}Ga_{0.7}As$ layers. However, it can not be seen that the islands are connected each other.

Figure 4.12 shows a typical L-I characteristic of this LED under dc condition at room-temperature. The insets in Fig. 4.12 show a top-viewed electroluminescence (EL) topograph and an emission spectrum of this LED. It is found that the light is emitted from each GaAs island. This LED was operated up to 27 μW at 190 mA, and the light output power increased linearly with increasing current up to 21 μW at 130 mA. At higher current, however, it was saturated because of thermal heating. This tendency was confirmed by the fact that the output power increased linearly up to higher current without saturation under pulsed (0.2 μs pulses at 5 kHz repetition

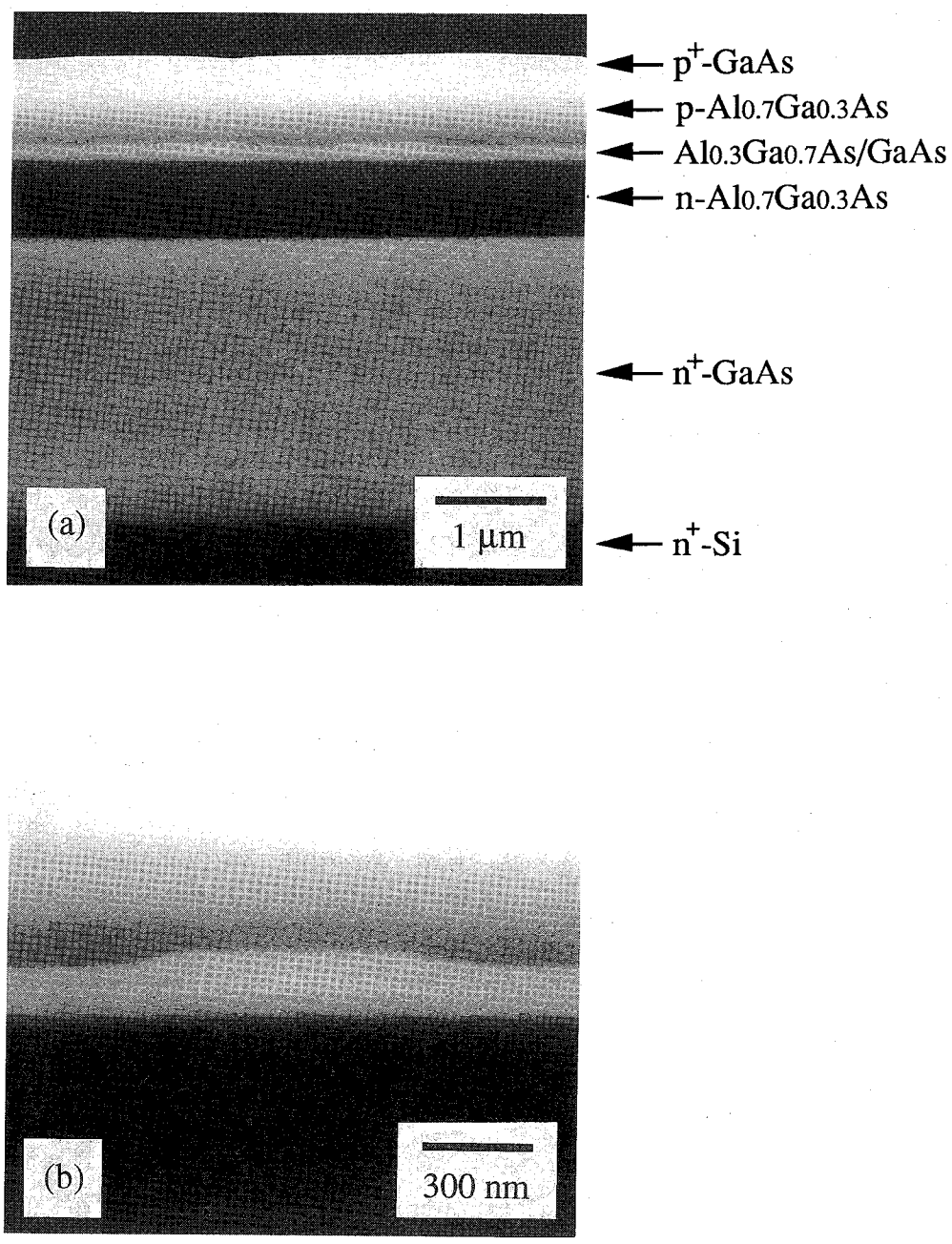


Fig. 4.11. Cross-sectional SEM micrographs: (a) overall AlGaAs/GaAs LED on Si with self-formed GaAs islands active region and (b) magnified GaAs island active region.

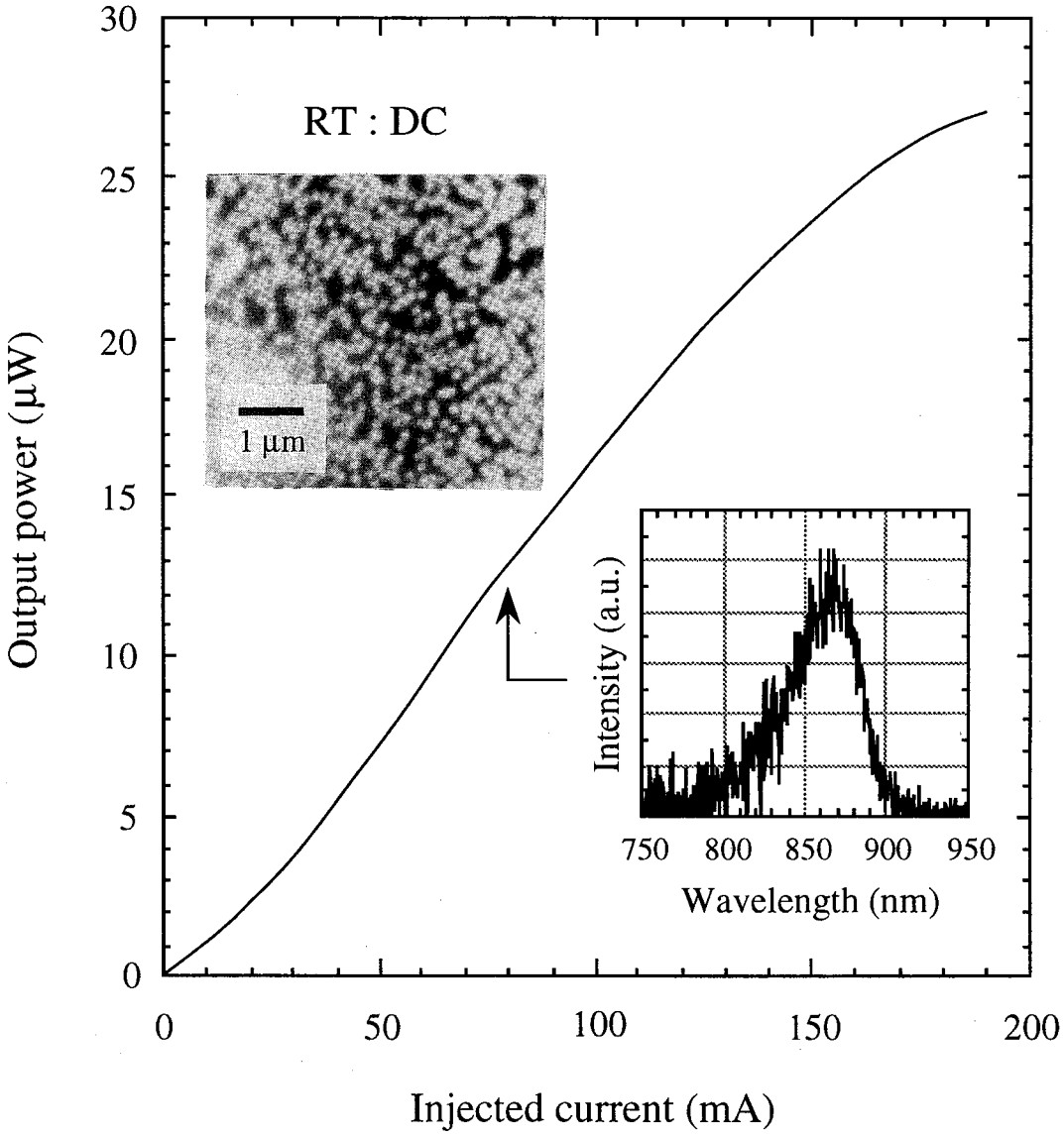


Fig. 4. 12. Typical L-I characteristic of the LED on Si under dc condition at room-temperature. The insets show a top-viewed EL topograph and an emission spectrum of this LED.

rate) operation. The peak emission wavelength at 80 mA was 868 nm and the full width at half maximum (FWHM) was 49 nm. An AlGaAs/GaAs LED on Si with a 9-nm-thick GaAs quantum well active region was also prepared as a reference. The structure of this LED was the same as that of an LED with the islands active region except for the active region structure. The output power of the LED with the islands active region decreased by ~1/10 of that of the LED with a quantum well active region due to the reduction in the size of the active region. From this result, however, it can be estimated that the output power density in the active region of the LED with the islands is about twice as high as that of the LED with a quantum well at the same injected current. This indicates that the high-quality GaAs islands could be successfully formed on Si. In addition, considering the island size and density, the dislocation number of the LED with the islands active region is estimated to be reduced to ~1/100 of that of the LED with a quantum well active region.

In order to investigate the reliability of the LED on Si with GaAs islands active region, the automatic current control (ACC) aging test was carried out under room-temperature dc condition at a constant current of 60 mA (0.5 $kA/cm^2$). This test was also carried out for an LED on Si with a quantum well active region. Figure 4.13 shows a typical degradation data under ACC aging tests of these LEDs. As shown in Fig. 4.13, the LED with a quantum well showed a rapid degradation in which the output power decreased rapidly to a half of the initial value only in a few minutes. In contrast, the output power of LED with the islands decreased very slowly and reached to a half of the initial value after ~14 hours in spite of the higher output power density in the active region. In particular, it should be noted that the decrease in the output power

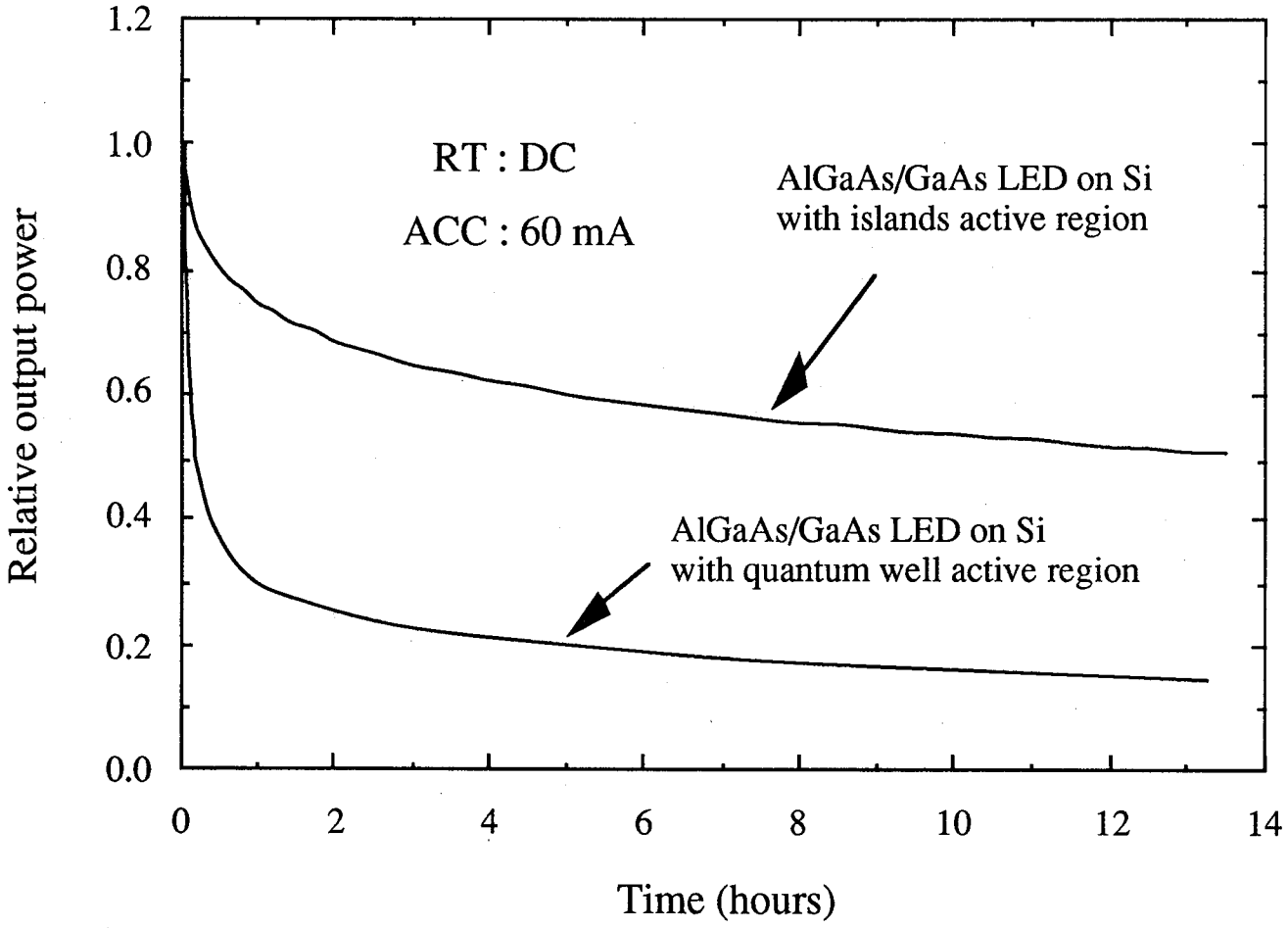


Fig. 4.13. Typical degradation data under ACC aging tests at room-temperature of the LEDs on Si with the islands active region and with a conventional quantum well active region.

of the LED with the islands is much more suppressed than that of the LED with a quantum well at the initial degradation stage within few minutes.

In order to study in detail the differences of degradation in these LEDs, EL observations were carried out on 10-μm-wide stripe contact laser structures fabricated from the same each LED wafer. The fabrication of these laser structures has been described in section 2.2. Figure 4.14 shows top-viewed EL topographs of progressive degradation stages of a laser structure with the islands active region at 20 °C. The injected current density during this observation was 0.5 kA/cm$^2$. For a laser structure with a quantum well, the EL topographs have been shown in Fig. 2.9. In the laser structure with a quantum well, a few <100> DLDs originating from the threading dislocations were generated and rapidly extended toward the center of the stripe[2]. On the other hand, it was observed that the DLDs growth was suppressed and only two bright spots (arrows shown in Fig. 4.14(a)) emitted from the islands vanished after 30 min in the laser structure with the islands [Fig. 4.14(b)]. At the subsequent degradation stage after 60 min, the degradation seems not to progress so fast because no change was observed on the EL topograph [Fig. 4.14(c)]. In the more progressive degradation stage, it was observed that almost bright spots gradually darkened. Figure 4.14 probably indicates that most of the islands (except these islands marked by arrows as shown in Fig. 4.14(a)) could avoid the threading dislocations and nonradiative recombination at the dislocations was drastically reduced by the confinement of the injected carriers in the islands. This resulted in improving the initial degradation as shown in Fig. 4.13. The subsequent slow degradation as shown in Fig. 4.13 is thought to be caused by the darkened islands probably due to gradual condensation of point

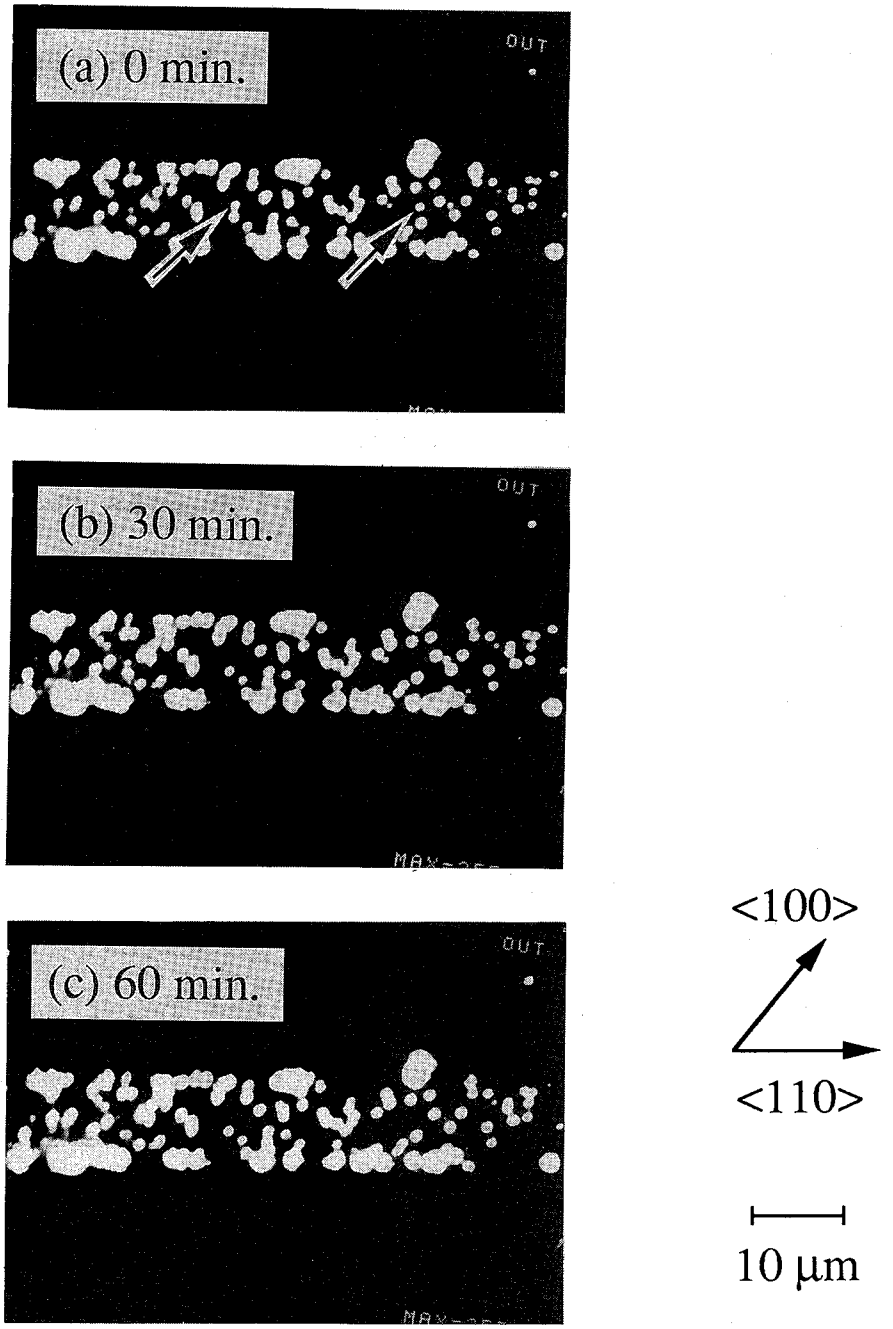


Fig. 4.14. Typical EL topographs of the laser structrure on Si with the islands active region after (a) 0, (b) 30 and (c) 60 min under dc operation at a constant current density of 0.5 kA/cm$^2$ and temperature of 20 °C.

defects in the islands. After all, this improved reliability is believed to have been caused by low dislocation numbers and suppressed <100> DLD growth in the active region due to reduction in the size of the active region.

## 4.4 Conclusions

The successful fabrication of an AlGaAs/GaAs quantum wire-like laser on Si with vertically-stacked quasi GaAs quantum wires was described. It was confirmed that the GaAs quantum wires of size (11-15 nm)×(83-127 nm) were grown on a V-grooved GaAs/Si substrate. Furthermore, the extremely low-threshold current (9.8 mA) AlGaAs/GaAs quantum wire-like laser on Si, which has the vertically-stacked quantum wires of size (20-21 nm)×(100-260 nm), was also demonstrated.

The fabrication of an AlGaAs/GaAs LED on Si with self-formed GaAs islands active region was also presented. The GaAs island size and density could be controlled by the TMG flow rate. At the TMG flow rate of 10 sccm and time of 6 s, the islands showed the conical shape with the heights of 90-170 nm, the diameters of 600-750 nm and the density of $1\text{-}2\times10^{7}$ $cm^{-2}$. This LED could be operated under dc condition at room-temperature. The reliability of this LED was much superior to that of an LED with a quantum well active region because of low dislocation numbers and suppressed DLD growth due to reduction of the active region by use of the small GaAs island structure.

References


1) Y. Hasegawa, T. Egawa, T. Jimbo and M. Umeno, Jpn. J. Appl. Phys., **34**, 2994 (1995).

2) E. A. Fitzgerald, J. Vac. Sci. Technol., B **7**, 782 (1989).

3) E. Kapon, S. Simhony, R. Bhat and D. M. Hwang, Appl. Phys. Lett., **55**, 2715 (1989).

4) E. Kapon, S. Simhony, J. P. Harbison, L. T. Florez and P. Worland, Appl. Phys. Lett., **56**, 1825 (1990).

5) E. Kapon, Proc. IEEE, **80**, 398 (1992).

6) E. Kapon, D. M. Hwang and R. Bhat, Phys. Rev. Lett., **63**, 430 (1989).

7) S. Simhony, E. Kapon, E. Colas, R. Bhat, N. G. Stoffel and D. M. Hwang, IEEE Photon. Technol. Lett., **2**, 305 (1990).

8) S. Simhony, E. Kapon, E. Colas, D. M. Hwang, N. G. Stoffel and P. Worland, Appl. Phys. Lett., **59**, 2225 (1991).

9) R. Bhat, E. Kapon, S. Simhony, E. Colas, D. M. Hwang, N. G. Stoffel and M. A. Koza, J. Cryst. Growth, **107**, 716 (1991).

10) E. Kapon, D. M. Hwang, M. Walther, R. Bhat and N. G. Stoffel, Surf. Sci., **267**, 593 (1992).

11) E. Kapon, K. Kash, E. M. Clausen, Jr., D. M. Hwang and E. Colas, Appl. Phys. Lett., **60**, 477 (1992).

12) M. Walther, E. Kapon, J. Christen, D. M. Hwang and R. Bhat, Appl. Phys. Lett., **60**, 521 (1992).

13) J. Christen, E. Kapon, M. Grundmann, D. M. Hwang, M. Joschko and D. Bimberg, Phys. Stat. Sol., **173**, 307 (1992).

14) J. Christen, E. Kapon, E. Colas, D. M. Hwang, L. M. Schiavone, M. Grundmann and D. Bimberg, Surf. Sci., **267**, 257 (1992).

15) E. Kapon, M. Walther, J. Christen, M. Grundmann, C. Caneau, D. M. Hwang, E. Colas, R. Bhat, G. H. Song and D. Bimberg,

Superlattices and Microstructures, **12**, 491 (1992).

16) N. Koguchi, S. Takahashi and T. Chikyow, J. Cryst. Growth, **111**, 688 (1991).

17) T. Ueda, Q. Z. Gao, E. Yamaichi, C. Yamagishi and M. Akiyama, J. Cryst. Growth, **145**, 707 (1994).

18) D. Leonard, M. Krishnamurthy, C. M. Reaves, S. P. Denbaars and P. M. Petroff, Appl. Phys. Lett., **63**, 3203 (1993).

19) D. Leonard, S. Fafard, K. Pond, Y. H. Zhang, J. L. Merz and P. M. Petroff, J. Vac. Sci. Technol., B **12**, 2516 (1994).

20) J. Oshinowo, M. Nishioka, S. Ishida and Y. Arakawa, Appl. Phys. Lett., **65**, 1421 (1994).

21) P. Chen, Q. Xie, A. Madhukar, Li Chen and A. Konkar, J. Vac. Sci. Technol., B **12**, 2568 (1994).

22) R. Leon, P. M. Petroff, D. Leonard and S. Fafard, Science, **267**, 1966 (1995).

23) S. Ruvimov, P. Werner, K. Scheerschmidt, U. Gosele, J. Heydenreich, U. Richter, N. N. Ledentsov, M. Grundmann, D. Bimberg, V. M. Ustinov, A. Yu. Egorov, P. S. Kop'ev and Zh. I. Alferov, Phys. Rev., B **51**, 14766 (1995).

24) D. S. L. Mui, D. Leonard, L. A. Coldren and P. M. Petroff, Appl. Phys. Lett., **66**, 1620 (1995).

25) M. Kitamura, M. Nishioka, J. Oshinowo and Y. Arakawa, Appl. Phys. Lett., **66**, 3663 (1995).

26) Qianghua Xie, P. Chen, A. Kalburge, T. R. Ramachandran, A. Nayfonov, A. Konkar and A. Madhukar, J. Cryst. Growth, **150**, 357 (1995).

27) R. Notzel, T. Fukui, H. Hasegawa, J. Temmyo and T. Tamamura, Appl. Phys. Lett., **65**, 2854 (1994).

28) R. Notzel, J. Temmyo and T. Tamamura, Nature, **369**, 131 (1994).

29) R. Notzel, J. Temmyo and T. Tamamura, Jpn. J. Appl. Phys., **33**,

L275 (1994).

30) R. Notzel, J. Temmyo, H. Kamada, T. Furuta and T. Tamamura, Appl. Phys. Lett., **65**, 457 (1994).

31) R. Notzel, J. Temmyo, T. Tamamura, T. Fukui and H. Hasegawa, Jpn. J. Appl. Phys., **34**, L872 (1995).

32) N. Kirstaedter, N. N. Ledentsov, M. Grundmann, D. Bimberg, V. M. Ustinov, S. S. Ruvimov, M. V. Maximov, P. S. Kop'ev, Zh. I. Alferov, U. Richter, P. Werner, U. Gosele and J. Heydenreich, Electron. Lett., **30**, 1416 (1994).

33) J. Temmyo, E. Kuramochi, M. Sugo, T. Nishiya, R. Notzel and T. Tamamura, Electron. Lett., **31**, 209 (1995).

34) D. Bimberg, N. N. Ledentsov, N. Kirstaedter, O. Schmidt, M. Grundmann, V. M. Ustinov, A. Yu. Egorov, A. E. Zhukov, M. V. Maximov, P. S. Kop'ev, Zh. I. Alferov, S. S. Ruvimov, U. Gosele and J. Heydenreich, *Extended Abstracts of the 1995 Int. Conf. Solid State Devices and Materials* (Osaka, 1995) p. 716.

35) Y. Hasegawa, T. Egawa, T. Jimbo and M. Umeno, J. Cryst. Growth, **145**, 728 (1994).

36) Y. Hasegawa, T. Egawa, T. Jimbo and M. Umeno, *Extended Abstracts of the 1995 Int. Conf. Solid State Devices and Materials* (Osaka, 1995) p. 722.

37) S. D. Hersee, E. Barbier and R. Blondeau, J. Cryst. Growth, **77**, 310 (1986).

38) Y. Hasegawa, T. Egawa, T. Jimbo and M. Umeno, Jpn. J. Appl. Phys., **32**, 509 (1993).

39) Y. Hasegawa, T. Egawa, T. Jimbo and M. Umeno, Jpn. J. Appl. Phys., **32**, L997 (1993).

40) Y. Hasegawa, T. Egawa, T. Jimbo and M. Umeno, *14th IEEE Int. Semiconductor Laser Conf. Digest* (Maui, 1994) p. 75.

41) H. K. Choi, C. A. Wang and J. C. C. Fan, J. Appl. Phys., **68**,

1916 (1990).

42) J. P. van der Ziel and N. Chand, J. Appl. Phys., **68**, 2731 (1990).

43) H. K. Choi, C. A. Wang and N. H. Karam, IEEE Photon. Technol. Lett., **3**, 289 (1991).

44) H. K. Choi, C. A. Wang and N. H. Karam, Appl. Phys. Lett., **59**, 2634 (1991).

45) T. Egawa, Y. Hasegawa, T. Jimbo and M. Umeno, Jpn. J. Appl. Phys., **31**, 791 (1992).

46) Y. H. Lo, R. Bhat, D. M. Hwang, C. Chua and C. -H. Lin, Appl. Phys. Lett., **62**, 1038 (1993).

47) M. Tachikawa, T. Yamada, T. Sasaki, H. Mori and Y. Kadota, Jpn. J. Appl. Phys., **34**, L657 (1995).

48) E. I. Givargizov, J. Cryst. Growth, **31**, 20 (1975).

49) K. Hiruma, M. Yazawa, T. Katsuyama, K. Ogawa, K. Haraguchi, M. Koguchi and H. Kakibayashi, J. Appl. Phys., **77**, 447 (1995).

50) T. Sato, K. Hiruma, M. Shirai, K. Tominaga, K. Haraguchi, T. Katsuyama and T. Shimada, Appl. Phys. Lett., **66**, 159 (1995).

51) T. Egawa, Y. Hasegawa, T. Jimbo and M. Umeno, IEEE Photon. Technol. Lett., **6**, 681 (1994).